Method for obtaining upper bounds on photonic band gaps

Mikael C. Rechtsman[1] and Salvatore Torquato[2,3,4,5]
[1]*Courant Institute of Mathematical Sciences, 251 Mercer Street, New York, New York 10012, USA*
[2]*Department of Chemistry, Princeton University, Princeton, New Jersey 08544, USA*
[3]*Princeton Center for Theoretical Physics, Princeton, New Jersey 08544, USA*
[4]*Program in Applied and Computational Mathematics, Princeton Institute for the Science and Technology of Materials, Princeton, New Jersey 08544, USA*
[5]*School of Natural Sciences, Institute for Advanced Study, Princeton, New Jersey 08544, USA*
(Received 26 June 2009; published 19 October 2009)

We present a method to calculate upper bounds on the photonic band gaps of two-component photonic crystals. The method involves calculating both upper and lower bounds on the frequency bands for a *given* structure, and then maximizing over all possible two-component structures. We apply this method to a number of examples, including a one-dimensional photonic crystal (or "Bragg grating") and two-dimensional photonic crystals (in both the TM and TE polarizations) with both four and sixfold rotational symmetries. We compare the bounds to band gaps of numerically optimized structures and find that the bounds are extremely tight. We prove that the bounds are "sharp" in the limit of low dielectric contrast ratio between the two components. This method and the bounds derived here have important implications in the search for optimal photonic band-gap structures.

DOI: 10.1103/PhysRevB.80.155126 PACS number(s): 42.70.Qs, 72.80.Tm

I. INTRODUCTION

Photonic crystals are structures that have a dielectric constant that is a periodic function of space. Ever since they were proposed independently by John[1] and Yablonovitch,[2] an enormous amount of research has gone into understanding their physical properties and developing their technological potential, from both experimental and theoretical perspectives. Perhaps the most important physical feature that photonic crystals can possess is a complete photonic band gap:[3] a range of frequencies for which no electromagnetic wave may propagate through the structure in any direction. This crucial characteristic allows the waves to be manipulated in a highly controlled way. To wit, one key application of photonic band-gap-possessing materials is near-lossless waveguiding, even around sharp bends.[4] Furthermore, these materials may be used to inhibit spontaneous emission,[2] provide waveguides for laser surgery,[5] and may in the future be the basis of all-optical chip integration.[6]

A large number of structures with complete photonic band gaps have been put forward, and many have been constructed. The first such three-dimensional example was a diamond structure of dielectric spheres;[7] many structures that have been proposed since are variants on this one. The inverse opal structure has a relatively small gap, but at frequencies that are sufficiently high that small manufacturing defects may suppress it. There are a plethora of others, including "Yablonovite," a structure that can be manufactured by drilling into a dielectric material in prescribed directions[8] and the "Woodpile" structure, manufactured by layering rectangular columns of dielectric material.[9] These are all materials composed of two dielectric components. The largest known band gap of any two-component structure in three dimensions is roughly 30%, relative to the center frequency, when the ratio between the two dielectric components (dielectric contrast) is 13, for a diamond lattice structure with nearest neighbors connected by cylindrical rods.[10] Since many applications require large photonic band gaps, the search for such structures has been extensive, and is ongoing.

There have been a number of systematic attempts to find two-component structures that yield maximal band gaps. In one of the first such studies, Maldovan *et al.*[11] proposed dielectric structures for each of the 11 face-centered cubic (fcc) space groups, and calculated their band gaps. The choice of the fcc space groups was well motivated, since the space group of the diamond lattice (space group $Fd\bar{3}m$, in international notation) is among these; however, their structures were not subjected to structural optimization of the band gap. A number of recent studies have applied different structural optimization techniques to find structures that maximize the photonic band gap in two dimensions for photonic crystals[12,13] and quasicrystals.[14] Different numerical techniques were used in these studies to evolve an initial guess of the structure it reaches a structure with the largest possible band gap. Thus far, these types of optimizations have been limited to two-dimensional systems due to the great computational cost of carrying out such a procedure in three dimensions.[15]

In this paper, we propose a method for finding upper bounds on the photonic band gap of two-component photonic crystals with dielectric constants ε_1 and ε_2 as a function of the dielectric contrast ratio, $\varepsilon_2/\varepsilon_1$. In order to demonstrate how this method is used, we apply it to derive upper bounds on band gaps in one-dimensional systems and two-dimensional systems with hexagonal symmetry and with square symmetry [in both the transverse-magnetic (TM) and transverse-electric (TE) polarizations]. In these examples, the bounds are on the gap between the first and second frequency bands, but the method can be generalized to obtain bounds on gaps between higher bands. We will report upper bounds for three-dimensional structures in a companion paper.[16] Given the extensive work on finding large-band-gap

structures, obtaining upper bounds is a highly germane contribution in that it sets the absolute limit on the possible band gap that may be obtained for any dielectric contrast. Importantly, if such an upper bound is realized, then it must be an optimal structure.

In order to obtain a bound on the band gap, we need both upper bounds and lower bounds on the frequency bands, which are the allowed frequencies of propagation at any Bloch wave vector, $\mathbf{k}$. The photonic band structure is found by solving an infinite-dimensional eigenvalue problem at any $\mathbf{k}$, and so to obtain upper bounds on the bands, we use a Rayleigh-Ritz procedure.[17] Lower bounds are obtained by the use of the method of intermediate problems.[18] The combination of upper and lower bounds yields a bound on the band gap *for a particular dielectric structure*. We place a bound on the band gap *over all structures* by maximizing the aforementioned bound over all possible two-component dielectric structures. By comparing the upper bounds we derive with the band gaps of known large-band-gap structures, we show that the bounds are extremely tight at low dielectric contrast. As the dielectric contrast increases, the bounds diverge slightly from the band gaps of the known maximum-band-gap structures, but still remain tight for the highest contrasts commonly used in fabrication of photonic crystals (roughly 10–13 for semiconductors such as GaAs or Si in air). We show in an Appendix that in the limit in which the dielectric contrast goes to 1, the lower bounds and upper bounds converge at any given $\mathbf{k}$.

The outline of this paper is as follows. We introduce the problem of calculating photonic band structure in Sec. II, and describe the methods used to calculate upper and lower bounds for the frequency bands in Secs. III A and III B, respectively. In Sec. III C, we discuss how these bounds on the frequency bands are combined to give overall bounds on the band gap for any structure at any fixed dielectric contrast. In Sec. IV we introduce realizability conditions for the Fourier components of indicator functions that serve to tighten the band-gap upper bounds. In Secs. V and VI, we apply our results to find the first band-gap upper bounds in one dimension and two dimensions (in the transverse-electric and transverse-magnetic polarizations), respectively. We close with concluding remarks in Sec. VII.

II. BASIC THEORETICAL BACKGROUND

The time-harmonic Maxwell's equations in a periodic, lossless, nonmagnetic medium with two components of dielectric constants ε_1 and ε_2 may be reduced to a wave equation on $\mathcal{R}^3$ in terms of the magnetic field, $\mathbf{H}$

$$\nabla \times \left[\frac{1}{\varepsilon(\mathbf{x})} \nabla \times \mathbf{H}(\mathbf{x}) \right] = \left(\frac{\omega}{c} \right)^2 \mathbf{H}(\mathbf{x}), \tag{1}$$

where $\varepsilon(\mathbf{x})$ is a periodic function that gives the dielectric constant as a function of position, $\mathbf{x}$, ω is the oscillation frequency of the wave, and c is the speed of light. The unit cell of this periodic structure is defined by primitive lattice vectors $\mathbf{a}_i$, $i=1,2,3$. The magnetic field must also be divergence free

$$\nabla \cdot \mathbf{H}(\mathbf{x}) = 0. \tag{2}$$

The dielectric function may be written as

$$\varepsilon(\mathbf{x}) = \varepsilon_1 \mathcal{I}_1(\mathbf{x}) + \varepsilon_2 \mathcal{I}_2(\mathbf{x}), \tag{3}$$

where $\mathcal{I}_i(\mathbf{x})$, called the indicator function for phase i, is 1 when $\mathbf{x}$ lies within phase i and is 0 otherwise.[19] The volume fraction for phase i is given by

$$\phi_i \equiv \frac{1}{V_{cell}} \int_{cell} \mathcal{I}_i(\mathbf{x}) d\mathbf{x}, \tag{4}$$

where V_{cell} is the volume of the periodic unit cell and the integral is carried out over that cell. Without loss of generality, we assume that $\varepsilon_2 \geq \varepsilon_1$. The wave equation may also be written in terms of the electric field in the medium, $\mathbf{E}$

$$\nabla \times \nabla \times \mathbf{E}(\mathbf{x}) = \varepsilon(\mathbf{x}) \left(\frac{\omega}{c} \right)^2 \mathbf{E}(\mathbf{x}), \tag{5}$$

where $\mathbf{E}$ must satisfy the no-free-charge constraint

$$\nabla \cdot [\varepsilon(\mathbf{x}) \mathbf{E}(\mathbf{x})] = 0. \tag{6}$$

According to Bloch's theorem, a complete set of solutions to both Eqs. (1) and (5) may be written as periodic vector fields modulated by a plane wave of wave vector $\mathbf{k}$, for all $\mathbf{k}$ within the first Brillouin zone of the lattice. We refer to $\mathbf{k}$ as the Bloch wave vector. We may thus write the fields as

$$\mathbf{H}(\mathbf{x}) = \exp(i\mathbf{k} \cdot \mathbf{x}) \mathbf{H}_{\mathbf{k}}(\mathbf{x}), \quad \mathbf{E}(\mathbf{x}) = \exp(i\mathbf{k} \cdot \mathbf{x}) \mathbf{E}_{\mathbf{k}}(\mathbf{x}), \tag{7}$$

where $\mathbf{H}_{\mathbf{k}}$ and $\mathbf{E}_{\mathbf{k}}$ are periodic vector fields with the same periodicity as $\varepsilon(\mathbf{x})$. Inserting Eq. (7) into Eqs. (1) and (5) gives

$$\begin{aligned} &(i\mathbf{k} + \nabla) \times \left[\frac{1}{\varepsilon(\mathbf{x})} (i\mathbf{k} + \nabla) \times \mathbf{H}_{\mathbf{k}}(\mathbf{x}) \right] \\ &\quad \equiv \Theta_{\mathbf{k}}(\mathbf{x}) \mathbf{H}_{\mathbf{k}}(\mathbf{x}) = \left(\frac{\omega}{c} \right)^2 \mathbf{H}_{\mathbf{k}}(\mathbf{x}), \end{aligned} \tag{8}$$

and

$$\begin{aligned} &(i\mathbf{k} + \nabla) \times [(i\mathbf{k} + \nabla) \times \mathbf{E}_{\mathbf{k}}(\mathbf{x})] \\ &\quad \equiv \Xi_{\mathbf{k}}(\mathbf{x}) \mathbf{E}_{\mathbf{k}}(\mathbf{x}) = \varepsilon(\mathbf{x}) \left(\frac{\omega}{c} \right)^2 \mathbf{E}_{\mathbf{k}}(\mathbf{x}), \end{aligned} \tag{9}$$

where the linear operators $\Theta_{\mathbf{k}}$ and $\Xi_{\mathbf{k}}$, defined by Eqs. (8) and (9), are Hermitian and positive definite for $\mathbf{k} \neq 0$, and positive semidefinite for $\mathbf{k}=0$. Equations (8) and (9) are linear eigenvalue problems (the latter being a generalized eigenvalue problem due to the nontrivial operator multiplying the field $\mathbf{E}_{\mathbf{k}}$ on the right-hand side) over the space of periodic fields, which we label $\mathcal{P}$. The divergence-free constraint for the magnetic field restricts the space over which Eq. (8) is solved to a subspace of $\mathcal{P}$; since this subspace is $\mathbf{k}$ dependent, we call it $\mathcal{P}_{\mathbf{k}}^H$. Similarly, the electric field must satisfy the no-free-charge constraint, and we call the subspace of $\mathcal{P}$ that has this property $\mathcal{P}_{\mathbf{k}}^E$. The operator ε is positive definite. We may explicitly write a plane-wave basis for the space $\mathcal{P}_{\mathbf{k}}^H$ as $\Delta_{\mathbf{k}} \equiv \{|\mathbf{k}, \mathbf{G}, \hat{\mathbf{e}}_{\mathbf{k}+\mathbf{G},\lambda}\rangle, \mathbf{G} \in \mathcal{G}, \lambda = 1,2\}$, where $|\mathbf{k}, \mathbf{G}, \hat{\mathbf{e}}_{\mathbf{k}+\mathbf{G},\lambda}\rangle$ represents a wave function given in the position representa-

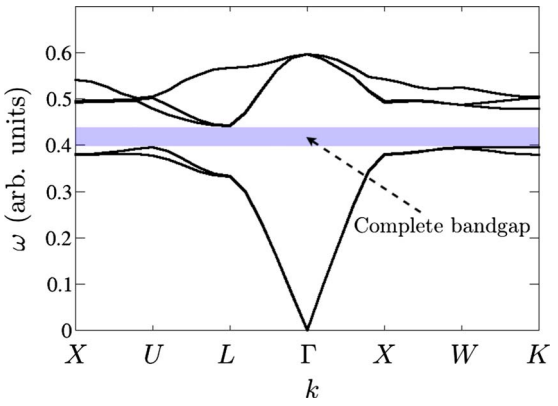

FIG. 1. (Color online) Band structure of a diamond lattice of high dielectric spheres (with the spheres in contact), at dielectric contrast $\varepsilon_2/\varepsilon_1=11.56$, at volume fraction $\phi_2=50\%$, as calculated in the MPB program (Ref. 20). In a band-structure diagram such as this one, the frequency for each band is plotted against wave vector in the first Brillouin zone. The shaded region is a complete photonic band gap, a range of frequencies for which there is no corresponding Bloch wave vector. The band gap is between the second and third frequency bands. The points X, U, L, Γ, W, and K denote special wave vectors of high symmetry in the Brillouin zone.

tion by $\hat{\mathbf{e}}_{\mathbf{k}+\mathbf{G},\lambda}\exp(i\mathbf{G}\cdot\mathbf{x})$ and $\mathcal{G}$ is the set of reciprocal lattice vectors of the lattice defined by the $\mathbf{a}_i$'s. Here, for every $\mathbf{G}$, the vectors $\hat{\mathbf{e}}_{\mathbf{k}+\mathbf{G},1}$, $\hat{\mathbf{e}}_{\mathbf{k}+\mathbf{G},2}$, and $\mathbf{k}+\mathbf{G}$ are constrained to form an orthogonal triad in order to satisfy the divergence-free constraint, Eq. (2).

The eigenvalues of the operator $\Theta_{\mathbf{k}}$ are given by $[\omega_i(\mathbf{k})/c]^2$, for $i=1,\ldots,\infty$, where $\omega_i(\mathbf{k})$ is the ith frequency (listed in ascending order) at Bloch wave vector $\mathbf{k}$ for the dielectric configuration given by the function ε. The frequencies $\omega_i(\mathbf{k})$ as a function of $\mathbf{k}$ are called the *band structure*. The band structure for a diamond lattice of high-dielectric spheres is shown in Fig. 1. In a band structure diagram such as this one, the ith eigenvalue corresponds to the ith band. As indicated in the figure, the range of frequencies for which there is no corresponding $\mathbf{k}$ is called the *photonic band gap*; in order to have a complete band gap, it must persist for all $\mathbf{k}$ in the first Brillouin zone. A common definition of the band gap for the ith band, and that which will be used in this paper, is

$$\beta_i(\varepsilon) \equiv \frac{\omega_{i+1}^{(\min)} - \omega_i^{(\max)}}{(\omega_{i+1}^{(\min)} + \omega_i^{(\max)})/2}, \tag{10}$$

where β_i is a functional of ε since it depends on the dielectric configuration, and $\omega_i^{(\min)}=\min_{\mathbf{k}\in 1\mathrm{BZ}}\omega_i(\mathbf{k})$ (analogously for the maxima) and 1BZ denotes the first Brillouin zone.

The central goal of this paper is to obtain upper bounds on the band gap, β_i, regardless of the dielectric configuration of the unit-cell (or perhaps given the constraint that it satisfies certain symmetry properties). To this end, we must obtain upper and lower bounds on the frequency bands themselves and then perform a maximization over all possible ε to ensure that we obtain an upper bound on the band gap over all dielectric configurations. We discuss this procedure in the subsequent section.

III. RIGOROUS BOUNDS

A. Upper bounds on the frequency bands

In order to find upper bounds on the frequencies $\omega_i(\mathbf{k})$ at a particular Bloch wave vector $\mathbf{k}$, we employ the Rayleigh-Ritz method[17] as applied to the eigenvalue problems defined by Eqs. (8) and (9). The procedure to find upper bounds using the magnetic field wave equation (8) is different than that for the electric field wave equation (9), and we start by examining the former. We choose a set of n orthonormal wave functions, $\Phi_n=\{|\phi_i\rangle, i=1,\ldots,n, |\phi_i\rangle\in\mathcal{P}_{\mathbf{k}}^H\}$, which we refer to as "trial functions." We then diagonalize the operator $\Theta_{\mathbf{k}}$ restricted to the subspace spanned by these vectors; this is simply a matter of diagonalizing the matrix with elements $U_{ij}^H\equiv\langle\phi_i|\Theta_{\mathbf{k}}|\phi_j\rangle$, $i,j=1,\ldots,n$. This matrix is necessarily Hermitian and positive semidefinite since $\Theta_{\mathbf{k}}$ has these properties, and thus its eigenvalues, defined as $[u_i^H(\mathbf{k})/c]^2$, are real and non-negative. The Rayleigh-Ritz procedure tells us that these eigenvalues, when placed in ascending order, are upper bounds on the first n eigenvalues of the full eigenvalue problem: $\omega_i(\mathbf{k})\le u_i^H(\mathbf{k})$, $i=1,\ldots,n$. In the present case, it is natural to choose plane waves as the orthonormal trial wave functions $|\phi_i\rangle$, $i=1,\ldots,n$, so that $\Phi_n\subset\Delta_{\mathbf{k}}$. The matrix elements of U^H in the plane-wave basis are:

$$\begin{aligned} U^H_{(\mathbf{G}',\lambda')(\mathbf{G}\lambda)} &= \langle\mathbf{k},\mathbf{G}',\hat{\mathbf{e}}_{\mathbf{k}+\mathbf{G},\lambda'}|\Theta_{\mathbf{k}}|\mathbf{k},\mathbf{G},\hat{\mathbf{e}}_{\mathbf{k}+\mathbf{G},\lambda}\rangle \\ &= [(\mathbf{k}+\mathbf{G}')\times\hat{\mathbf{e}}_{\mathbf{k}+\mathbf{G}',\lambda'}]\cdot[(\mathbf{k}+\mathbf{G})\times\hat{\mathbf{e}}_{\mathbf{k}+\mathbf{G},\lambda}] \\ &\quad\times\frac{1}{V_{cell}}\int_{cell}d\mathbf{x}\frac{1}{\varepsilon(\mathbf{x})}\exp[i(\mathbf{G}-\mathbf{G}')\cdot\mathbf{x}]. \end{aligned} \tag{11}$$

The procedure to find upper bounds on $\omega_i(\mathbf{k})$ via the electric field wave equation is nearly identical to that for the magnetic field, except that due to the nontrivial operator ε on the right-hand side of Eq. (9), a different basis set must be chosen. We must choose a set of n vectors, $\{|\psi_i\rangle, i=1,\ldots,n, |\psi_i\rangle\in\mathcal{P}_{\mathbf{k}}^E\}$ (also called trial wave functions) with the property that $\langle\psi_i|\varepsilon|\psi_j\rangle=\delta_{ij}$ for $i,j=1,\ldots,n$. If certain vectors have this property, we say that they are orthonormal with respect to the function ε. Apart from this special choice of basis vectors, the procedure is similar to that of the magnetic field case, except that here we diagonalize the matrix U_{ij}^E with elements $U_{ij}^E\equiv\langle\psi_i|\Xi_{\mathbf{k}}|\psi_j\rangle$, $i,j=1,\ldots,n$. Thus, new upper bounds $[u_i^E(\mathbf{k})]$ are obtained, so that $\omega_i(\mathbf{k})\le u_i^E(\mathbf{k})$, $i=1,\ldots,n$.

The bounds obtained using the magnetic and electric field wave equations are different in general. This works to our advantage in placing tighter upper bounds on the band gap because for any given ε, we may take the lower of the two as an upper bound. Namely, we take

$$u_i(\mathbf{k}) = \min[u_i^H(\mathbf{k}), u_i^E(\mathbf{k})]. \tag{12}$$

B. Lower bounds on the frequency bands

Lower bounds on the bands may be found via the method of intermediate problems of the second type,[18] which was first applied to photonic systems by Vatsya and Nikumb.[21] In that work, bounds were calculated for particular dielectric

configurations of a unit cell but were not used to place a bound on the band gap over all possible configurations of the cell.

The method is described as follows: consider the Hermitian eigenvalue problem $\mathcal{H}|\lambda\rangle=\lambda|\lambda\rangle$ over an infinite-dimensional vector space, $\mathcal{V}$. Assume that $\mathcal{H}$ can be written as the sum of two linear operators,

$$\mathcal{H}=\mathcal{A}+\mathcal{B}, \tag{13}$$

where $\mathcal{A}$ is diagonal in a known, orthonormal basis set $\Phi=\{|\phi_i\rangle, i=1,\ldots,\infty\}$, and $\mathcal{B}$ is positive definite. Following Ref. 18, we may define a new inner product as $[\lambda|\mu]=\langle\lambda|\mathcal{B}|\mu\rangle$, where $|\lambda\rangle,|\mu\rangle\in\mathcal{V}$. Since the operator $\mathcal{B}$ is positive definite, it is necessarily Hermitian, so an orthonormal basis for the new inner product $[\cdot|\cdot]$ may be found. This basis, which we label $\{|p_i\rangle\}$, has the property $[p_i|p_j]=\delta_{ij}$ by definition.

For any $|\lambda\rangle\in\mathcal{V}$, we have from Bessel's inequality that

$$\langle\lambda|\mathcal{B}|\lambda\rangle=[\lambda|\lambda]\geq\sum_{i=1}^{n}|[\lambda|p_i]|^2=\sum_{i=1}^{n}|\langle\lambda|\mathcal{B}|p_i\rangle|^2, \tag{14}$$

where we have chosen a finite set of n of the $|p_i\rangle$'s. It follows that $\mathcal{B}\geq\sum_{i=1}^{n}\mathcal{B}|p_i\rangle\langle p_i|\mathcal{B}$ in the operator sense, and thus,

$$\mathcal{H}=\mathcal{A}+\mathcal{B}\geq\mathcal{A}+\sum_{i=1}^{n}\mathcal{B}|p_i\rangle\langle p_i|\mathcal{B}\equiv\mathcal{A}+\mathcal{B}_n\equiv\mathcal{H}_n, \tag{15}$$

where $\mathcal{B}_n$ and $\mathcal{H}_n$ are defined in Eq. (15) and we have that $\mathcal{H}_n\leq\mathcal{H}$, $\forall n\geq 1$. It is necessarily true that if the eigenvalues of $\mathcal{H}_n$ and $\mathcal{H}$ are listed in ascending order, the ith eigenvalue of $\mathcal{H}_n$ is a lower bound on the ith eigenvalue of $\mathcal{H}$.

The operator $\mathcal{H}_n$ can be expressed in the orthonormal basis Φ, after some algebraic manipulation, as

$$\mathcal{H}_n=\mathcal{A}+\sum_{i,j=1}^{n}(M^{-1})_{ij}|\phi_i\rangle\langle\phi_j|, \tag{16}$$

where a finite set of n orthonormal trial vectors, $\Phi_n=\{|\phi_i\rangle, i=1,\ldots,n\}$, have been chosen, and M is an $n\times n$ matrix with elements given by $M_{ij}=\langle\phi_i|\mathcal{B}^{-1}|\phi_j\rangle$.

For the magnetic field eigenvalue problem in Eq. (8), we separate the operator $\Theta_{\mathbf{k}}$ as follows:

$$\underbrace{\Theta_{\mathbf{k}}}_{\mathcal{H}}=\underbrace{(i\mathbf{k}+\nabla)\times\left[\frac{1}{\varepsilon_0}(i\mathbf{k}+\nabla)\times\right]}_{\mathcal{A}}+\underbrace{(i\mathbf{k}+\nabla)\times\left[\left(\frac{1}{\varepsilon(\mathbf{x})}-\frac{1}{\varepsilon_0}\right)(i\mathbf{k}+\nabla)\times\right]}_{\mathcal{B}} \tag{17}$$

Here, we introduce ε_0 and require it to have the property that $\varepsilon_0>\varepsilon_2\geq\varepsilon_1$. We choose a set of n plane waves as trial wave functions so that in this case, $\Phi_n\subset\Delta_{\mathbf{k}}$. Note that the first operator on the right-hand side of Eq. (17) is diagonal in the plane-wave basis $\Delta_{\mathbf{k}}$, and the second is necessarily positive definite as long as $\mathbf{k}\neq 0$. Therefore, all of the assumptions required for the application of the method of intermediate problems are met by this separation of $\Theta_{\mathbf{k}}$, as long as $\mathbf{k}\neq 0$.

In the plane-wave basis, the matrix elements of M may be shown to be

$$M_{(\mathbf{G}',\lambda')(\mathbf{G}\lambda)}=\frac{1}{|\mathbf{k}+\mathbf{G}'|^2|\mathbf{k}+\mathbf{G}|^2}[(\mathbf{k}+\mathbf{G}')\times\hat{\mathbf{e}}_{\mathbf{k}+\mathbf{G}',\lambda'}]\cdot[(\mathbf{k}+\mathbf{G})\times\hat{\mathbf{e}}_{\mathbf{k}+\mathbf{G},\lambda}]\frac{1}{V_{cell}}\times\int_{cell}d\mathbf{x}\left[\frac{1}{\varepsilon(\mathbf{x})}-\frac{1}{\varepsilon_0}\right]^{-1}\exp[i(\mathbf{G}-\mathbf{G}')\cdot\mathbf{x}]. \tag{18}$$

If we set $\mathcal{H}=\Theta_{\mathbf{k}}$ with the choice of $\mathcal{A}$ and $\mathcal{B}$ given in Eq. (17), and work with n plane waves in the set Φ_n, the eigenvalues of the operator $\mathcal{H}_n$, listed in ascending order, are simply $[l_i(\mathbf{k})/c]^2$ where $l_i(\mathbf{k})$ is the lower bound on the ith frequency band. In order to find the eigenvalues of $\mathcal{H}_n$, it is necessary to diagonalize an $n\times n$ matrix. It is important to note that $\mathcal{H}_n$ is an operator on the entire space $\mathcal{P}_{\mathbf{k}}^{H}$ and thus has an infinite number of eigenvalues; n of these will be in the subspace spanned by Φ_n and the rest will not. This fact places a constraint on the choice of ε_0 if we are to find the largest possible nontrivial lower bounds, $l_i(\mathbf{k})$, $i\leq n$. Indeed, ε_0 must be chosen such that $[l_i(\mathbf{k})/c]^2$ does not exceed the lowest eigenvalue of $\mathcal{H}_n$ corresponding to an eigenvector that is not in the space spanned by Φ_n. The greatest lower bound is obtained for the largest possible choice of ε_0 subject to this constraint.

C. Upper bounds on the band gap

In Secs. III A and III B, we have discussed how upper and lower bounds for the bands may be obtained at a given Bloch wave vector $\mathbf{k}$. Using these bounds, it is possible to bound the band gap from above. Assume for the moment that for a given set of Bloch wave vectors, $K=\{\mathbf{k}_j, j=1,\ldots,m\}$, $m\geq 1$, lower bounds $[l_i(\mathbf{k})]$ and upper bounds $[u_i(\mathbf{k})]$ may be obtained on all bands up to and including the nth, so that for $1\leq i\leq n$, $l_i(\mathbf{k})\leq\omega_i(\mathbf{k})\leq u_i(\mathbf{k})$.

It is clear that $\min_{\mathbf{k}\in K}u_i(\mathbf{k})\geq\omega_i^{(\min)}$ and $\max_{\mathbf{k}\in K}l_i(\mathbf{k})\leq\omega_i^{(\max)}$. It follows that:

$$\beta_i(\varepsilon)\leq\frac{\min_{\mathbf{k}\in K}u_{i+1}(\mathbf{k})-\max_{\mathbf{k}\in K}l_i(\mathbf{k})}{[\min_{\mathbf{k}\in K}u_{i+1}(\mathbf{k})+\max_{\mathbf{k}\in K}l_i(\mathbf{k})]/2}\equiv\gamma_i(\varepsilon). \tag{19}$$

The quantity $\gamma_i(\varepsilon)$, defined in Eq. (19), necessarily bounds the band gap from above. Note that $\gamma_i(\varepsilon)$ implicitly depends on the trial wave functions that are used at each $\mathbf{k}\in K$. As more wave vectors in the first Brillouin zone are included in K and the lower and upper bounds get closer to the true frequencies, the value of the band-gap bound approaches that of the band gap. The bound on the band gap for *any* dielectric structure is

$$\Gamma_i = \max_{\varepsilon} \gamma_i(\varepsilon), \tag{20}$$

subject to the constraint that $\varepsilon(\mathbf{x})$ may take on only two different values within the unit cell, ε_1 and ε_2. This constraint leads to much lower upper bounds on the band gap than would have been the case for *any* periodic function.

The maximization over dielectric structures described in Eq. (20) generalizes the bounds on the band gap for a particular structure to a bound over all structures (or those subject to some symmetry condition). The procedure used to carry out the maximization while constraining ε to have only two values may be described as follows. Observe that both the calculation of upper bounds (described in Sec. III A) and lower bounds (described in Sec. III B) on the frequency bands involve Fourier transforms of some function of ε. Indeed, for a given set of Bloch wave vectors, K, trial functions for each $\mathbf{k} \in K$, and dielectric constants ε_1 and ε_2, $\gamma_i(\varepsilon)$ may be written as a function of a finite number of Fourier components of the indicator functions $\mathcal{I}_1$ and $\mathcal{I}_2$. In fact, since the indicator functions have the property that $\mathcal{I}_1+\mathcal{I}_2=1$, $\gamma_i(\varepsilon)$ may be written in terms of the Fourier components of $\mathcal{I}_2$ only, which we label $\tilde{\mathcal{I}}_2(\mathbf{G})$, where $\mathbf{G}$ is a reciprocal lattice vector, and

$$\tilde{\mathcal{I}}_2(\mathbf{G}) = \frac{1}{V_{cell}} \int_{cell} d\mathbf{x} \exp(i\mathbf{G}\cdot\mathbf{x}) \mathcal{I}_2(\mathbf{x}). \tag{21}$$

Strong constraints may be placed on the $\tilde{\mathcal{I}}_2(\mathbf{G})$'s based on the realizability of the function $\mathcal{I}_2$. These constraints depend on the symmetry constraints imposed on ε, and will be discussed individually for a number of different cases in following sections. The maximization described in Eq. (20) is carried out over all *realizable* values of the $\tilde{\mathcal{I}}_2(\mathbf{G})$'s that arise in the calculation of the upper and lower bounds. In the following section, we discuss realizability conditions for these Fourier components.

IV. REALIZABILITY CONDITIONS DICTATED BY THE INDICATOR FUNCTION

In this section, we derive strong realizability conditions on the Fourier components $\tilde{\mathcal{I}}_2(\mathbf{G})$ in any spatial dimension d, given that they must give rise to indicator functions in real space. The problem of finding realizability conditions has been extensively studied in different contexts, notably for two-point correlation functions in multicomponent random systems.[19,22,23] These conditions are necessary in order to obtain the lowest possible upper bound for the band gap, as discussed in the previous section. We derive below three types of conditions that each serve to constrain the space of allowed Fourier components. We call these the "rearrangement" conditions, the Parseval conditions, and the Toeplitz conditions.

A. Rearrangement conditions

We may rewrite these Fourier components, for a given reciprocal lattice vector $\mathbf{G}$ as

$$\tilde{\mathcal{I}}_2(\mathbf{G}) = |\tilde{\mathcal{I}}_2(\mathbf{G})| \exp(i\theta_{\mathbf{G}}), \tag{22}$$

where $\theta_{\mathbf{G}}$ is the phase of the Fourier component at $\mathbf{G}$. This implies that

$$|\tilde{\mathcal{I}}_2(\mathbf{G})| = \frac{1}{V_{cell}} \int_{cell} d\mathbf{x} \mathcal{I}_2(\mathbf{x}) \cos(\mathbf{G}\cdot\mathbf{x} - \theta_{\mathbf{G}}), \tag{23}$$

where the integral here is carried out over the d-dimensional real-space unit cell. If $\mathbf{G}=0$, $\tilde{\mathcal{I}}_2(\mathbf{G})$ is simply the volume fraction of phase 2, ϕ_2, and thus we have that

$$0 \le \tilde{\mathcal{I}}_2(0) \le 1. \tag{24}$$

For all other reciprocal lattice vectors ($\mathbf{G} \neq 0$), we wish to find the maximum possible value of $|\tilde{\mathcal{I}}_2(\mathbf{G})|$ for a given phase, $\theta_{\mathbf{G}}$, and for a fixed volume fraction, ϕ_2

$$|\tilde{\mathcal{I}}_2(\mathbf{G})|^{(\max)} \equiv \max_{\mathcal{I}_2:\phi_2=const} |\tilde{\mathcal{I}}_2(\mathbf{G})|. \tag{25}$$

The quantity $|\tilde{\mathcal{I}}_2(\mathbf{G})|^{(\max)}$, implicitly a function of ϕ_2, is the largest possible Fourier amplitude that may be found at $\mathbf{G}$. The calculation of this quantity thus places a realizability condition on the Fourier component $\tilde{\mathcal{I}}_2(\mathbf{G})$. To find $|\tilde{\mathcal{I}}_2(\mathbf{G})|^{(\max)}$, we utilize the rearrangement theorem for functions.[24] It states that for any positive, bounded function f,

$$\max_{\mathcal{I}_2:\phi_2=const} \frac{1}{V_{cell}} \int_{cell} d\mathbf{x} f(\mathbf{x}) \mathcal{I}_2(\mathbf{x}) = \frac{1}{V_{cell}} \int_{cell} d\mathbf{x} f(\mathbf{x}) \mathcal{I}_2^{(\max)}(\mathbf{x}), \tag{26}$$

where

$$\mathcal{I}_2^{(\max)}(\mathbf{x}) = \begin{cases} 1, & \text{if } f(\mathbf{x}) > c, \\ 0, & \text{otherwise}, \end{cases} \tag{27}$$

and c is a constant that may be obtained from the constraint on the volume fraction, namely,

$$\phi_2 = \frac{1}{V_{cell}} \int_{cell} d\mathbf{x} \mathcal{I}_2^{(\max)}(\mathbf{x}). \tag{28}$$

This result holds for functions that may be negative as well. To prove this, we choose an f_0 which is less than $f(\mathbf{x})$ for all $\mathbf{x}$ in the cell. We may write

$$\max_{\mathcal{I}_2:\phi_2=const} \frac{1}{V_{cell}} \int_{cell} d\mathbf{x} f(\mathbf{x}) \mathcal{I}_2(\mathbf{x}) = \max_{\mathcal{I}_2:\phi_2=const} \left\{ \frac{1}{V_{cell}} \int_{cell} d\mathbf{x} [f(\mathbf{x}) - f_0] \mathcal{I}_2(\mathbf{x}) + f_0\phi_2 \right\}. \tag{29}$$

Since ϕ_2 is held fixed in the optimization, and $f(\mathbf{x})-f_0>0$ for all $\mathbf{x}$, Eq. (26) holds true. A perfectly analogous result holds for finding minima of expressions such as the one in Eq. (26), the only difference being that the ">" sign in Eq. (27) is replaced with a "<" sign. Using this result with $f(\mathbf{x})=\cos(\mathbf{G}\cdot\mathbf{x}-\theta_{\mathbf{G}})$ gives us an explicit way to evaluate the right-hand side of Eq. (25). This places strict bounds on

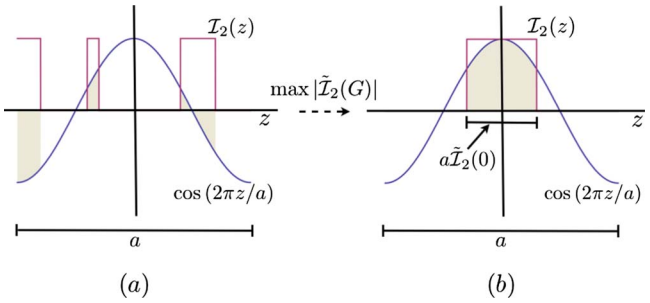

FIG. 2. (Color online) Depiction of how realizability conditions are imposed on $\tilde{\mathcal{I}}_2(G)$, with $G=2\pi/a$ and $\theta_G=0$. In (a), a general indicator function $\mathcal{I}_2(z)$ is plotted, where $z\in[-a/2,a/2]$, the one-dimensional real-space unit cell. The corresponding value of $\tilde{\mathcal{I}}_2(G)$ is equal to the shaded region (normalized by the period, a). In (b), phase 2 is grouped into a contiguous region; this yields the maximal $|\tilde{\mathcal{I}}_2(G)|$. Note that we assume that $\tilde{\mathcal{I}}_2(G)$ is real in (a); in (b), this is true by inversion symmetry. In both (a) and (b) the volume fraction of phase 2 is $\phi_2=\tilde{\mathcal{I}}_2(0)$.

$\tilde{\mathcal{I}}_2(\mathbf{G})$ as a function of $\theta_{\mathbf{G}}$ and ϕ_2. This procedure is depicted in Fig. 2, in a one-dimensional system with period a and using the reciprocal lattice vector $G=2\pi/a$ and phase $\theta_G=0$.

If we wish to enforce a certain point or space group symmetry on the structure, we may place even stronger realizability conditions on the Fourier components of the indicator functions. This will be the case in Secs. VI A and VI B, where we place bounds on the band gap of two-dimensional photonic crystals with sixfold rotational symmetry (C_6) and fourfold rotational symmetry (C_4), respectively.

Assume that we wish our structure to have the symmetry associated with some point group of symmetry operations, $\mathcal{S}$. We restrict ourselves to point group operations, as opposed to full space group operations. It follows that for any reciprocal lattice vector $\mathbf{G}$, we have that $\tilde{\mathcal{I}}_2(\mathbf{G})=\tilde{\mathcal{I}}_2(S\mathbf{G})$, where $S\in\mathcal{S}$ is a point group operation. We may use this to place a constraint on the Fourier amplitudes $|\tilde{\mathcal{I}}_2(\mathbf{G})|$: for structures with $\mathcal{S}$-point group symmetry enforced,

$$|\tilde{\mathcal{I}}_2(\mathbf{G})|^{(\max)} = \max_{\mathcal{I}_2:\phi_2=const} \frac{1}{V_{cell}} \times \int_{cell} d\mathbf{x}\left[\sum_{S\in\mathcal{S}} \cos(S\mathbf{G}-\theta_{\mathbf{G}})\right]\mathcal{I}_2(\mathbf{x}). \tag{30}$$

The result of this maximization may be evaluated using Eq. (26). If the point group $\mathcal{S}$ includes inversion, as do C_4 and C_6, then $\theta_{\mathbf{G}}=0$ for all $\mathbf{G}$. Figure 3 is a depiction of the integral that must be performed for Eq. (26) for the case of C_6 rotational symmetry in two dimensions. In this case, $f(\mathbf{x})=\Sigma_{S\in C_6}\cos(S\mathbf{G}\cdot x-\theta_{\mathbf{G}})$. Here, we take $\mathbf{G}$ to be in the first ring (a set of vectors with equal norm) of reciprocal lattice vectors away from the origin. Figure 4 explicitly shows the region of realizability for the Fourier amplitude $|\tilde{\mathcal{I}}_2(\mathbf{G})|$ for this case.

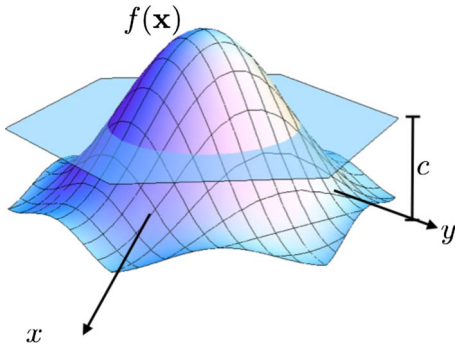

FIG. 3. (Color online) Schematic depiction of the integral in Eq. (30) for a two-dimensional system with C_6 symmetry imposed. The curve $f(\mathbf{x})=\Sigma_{S\in C_6}\cos(S\mathbf{G}\cdot\mathbf{x}-\theta_{\mathbf{G}})$ is plotted in a single hexagonal unit cell. The reciprocal lattice vector at which the Fourier transform is taken here is in the first ring of reciprocal lattice vectors away from the origin. The function $\mathcal{I}_2^{\max}(\mathbf{x})$ takes on the value 1 when $f(\mathbf{x})>c$ and is 0 otherwise. The integral must be carried out numerically for values of c within the range $\min_{\mathbf{x}} f(\mathbf{x})<c<\max_{\mathbf{x}} f(\mathbf{x})$.

B. Parseval conditions

Further realizability conditions may be imposed on the Fourier components by employing Parseval's theorem. It states that

$$\frac{1}{V_{cell}}\int_{cell} d\mathbf{x}\mathcal{I}_2^2(\mathbf{x}) = \sum_{\mathbf{G}\in\mathcal{G}} |\tilde{\mathcal{I}}_2(G)|^2. \tag{31}$$

Since $\mathcal{I}^2=\mathcal{I}$, it follows that

$$\phi_2(1-\phi_2) = \sum_{\mathbf{G}\in\mathcal{G}\setminus\{0\}} |\tilde{\mathcal{I}}_2(G)|^2. \tag{32}$$

The calculation of $\gamma_i(\varepsilon)$, the bound on the band gap for a particular dielectric structure, involves only a finite number of Fourier components $\tilde{\mathcal{I}}_2(\mathbf{G})$, the number of which depends on the number of trial functions used. If we only include a finite number of reciprocal lattice vectors, in the set $\mathcal{G}_S\subset\mathcal{G}$, it follows from Eq. (32) that we have the inequality:

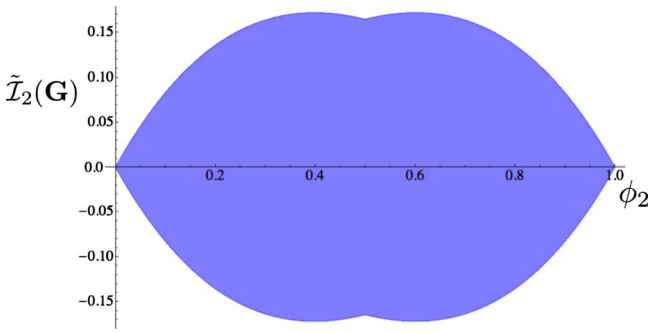

FIG. 4. (Color online) The shaded region is the space of realizable ordered pairs $[\phi_2,\tilde{\mathcal{I}}_2(\mathbf{G})]$, according to the rearrangement conditions, for a system with sixfold rotational symmetry imposed. Here, $\mathbf{G}$ is in the first ring of reciprocal lattice vectors away from the origin. Note that $\tilde{\mathcal{I}}_2(\mathbf{G})$ must be real, because of the imposed C_6 symmetry, which contains inversion.

$$\phi_2(1-\phi_2) \geq \sum_{\mathbf{G}\in\mathcal{G}_S\setminus\{0\}} |\tilde{\mathcal{I}}_2(G)|^2. \tag{33}$$

Relation (33) serves as an important realizability condition.

C. Toeplitz conditions

The indicator function $\mathcal{I}$ may be thought of as a linear operator on the space of functions whose domain is the unit cell. Choosing a set of n reciprocal lattice vectors, $\{\mathbf{G}_1,\ldots,\mathbf{G}_n\}=\mathcal{G}_S$, and defining the matrix $T(\mathcal{I}_2)$ by its elements

$$T_{jk}(\mathcal{I}_2) = \frac{1}{V_{cell}}\int_{cell} d\mathbf{x}\mathcal{I}_2(\mathbf{x})\exp\, i(\mathbf{G}_k-\mathbf{G}_j), \tag{34}$$

we see that T is a Toeplitz matrix with dimension n. It is well known[25] that for a Toeplitz matrix $T(f)$, where f is a bounded function that maps a unit cell to the real numbers, we must have that for each $j=1,\ldots,n$,

$$\min_{\mathbf{x}} f(\mathbf{x}) \leq \tau_j(f) \leq \max_{\mathbf{x}} f(\mathbf{x}), \tag{35}$$

where $\tau_j(f)$ is the jth eigenvalue of $T(f)$. Replacing f with $\mathcal{I}_2$ here gives us a new and quite strong realizability condition for the Fourier components of the indicator function. Thus, we have:

$$0 \leq \tau_j(\mathcal{I}_2) \leq 1. \tag{36}$$

These inequalities further constrain the space of realizable Fourier components by placing restrictions on the eigenvalues of the operator $T(\mathcal{I}_2)$.

V. UPPER BOUNDS ON THE FIRST BAND GAP IN ONE DIMENSION

In the case of a one-dimensional photonic crystal, we set the dielectric constant to be a periodic function of only a single spatial variable, z, so that $\varepsilon(\mathbf{x})\rightarrow\varepsilon(z)$. Thus, the configuration may be thought of as a series of slabs arranged periodically, with period a. The slabs are taken to be infinite in extent in the x and y directions. We constrain the direction of propagation to be only in the z direction, so that $\mathbf{k}=(0,0,k)$. This system is depicted in Fig. 5. Since there is a symmetry associated with rotations around the z axis, we only consider wave functions polarized along the x axis.

In this section, we discuss how the lower bounds $[l_i(\mathbf{k})]$ and upper bounds, $[u_i(\mathbf{k})]$ for the frequency bands are obtained. For the latter, both magnetic and electric field wave equations are employed since they lead to different upper bounds. We limit ourselves to bounding the band gap between the first and second bands in the spectrum, which means we must obtain lower bounds on the first frequency band and upper bounds on the second.

We choose a single Bloch wave vector given by $k=\pi/a$, at the Brillouin zone boundary, at which to calculate the lower and upper bounds. This is an obvious choice since it is typically the point at which the first and second bands are at their closest. The trial wave functions used for both the lower and upper bound procedures are plane waves polarized in the

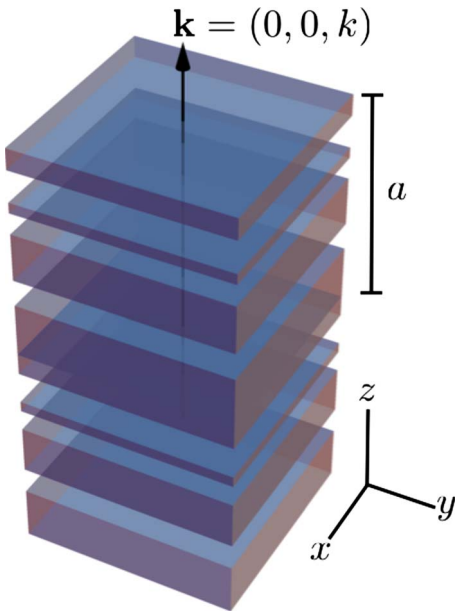

FIG. 5. (Color online) One-dimensional photonic crystal. Here, phase 2 (the high dielectric-constant phase) is represented by the translucent slabs and phase 1 is empty space. The structure is periodic in the z direction with period a and extends infinitely in the x and y directions. We limit our analysis to Bloch wave propagation along the z direction, thus $\mathbf{k}=(0,0,k)$.

x direction with wave vectors of the form $\mathbf{G}=(0,0,G)$. We take 6 such trial wave functions with $Ga=-6\pi$, -4π, -2π, 0, 2π, and 4π. Note that these trial wave functions satisfy both the divergence-free constraint [Eq. (2)] and the no-free-charge constraint [Eq. (6)]. Furthermore, they are orthonormal in the usual inner product and with respect to the dielectric constant function, which means that upper bounds may be obtained from both the magnetic and electric field wave equations. The lower bounds are obtained by diagonalizing the matrix $\mathcal{H}_n$, defined in Eq. (16), within the space spanned by the trial functions. The constant ε_0 is chosen such that the lowest of these eigenvalues is equal to the lowest eigenvalue of $\mathcal{H}_n$ that lies outside the space spanned by the trial wave functions (which is $49\pi^2/a^2$ in this case). Thus, for a given dielectric structure a bound on the first band gap $\gamma_1(\varepsilon)$ may be obtained.

In order to obtain an overall bound on the band gap, we must maximize $\gamma_1(\varepsilon)$ over all structural parameters that enter into this expression. With the choice of trial wave functions described in the previous paragraph, six Fourier components enter in, namely, $\tilde{\mathcal{I}}_2(0)$, $\tilde{\mathcal{I}}_2(2\pi/a)$, $\tilde{\mathcal{I}}_2(4\pi/a)$, $\tilde{\mathcal{I}}_2(6\pi/a)$, $\tilde{\mathcal{I}}_2(8\pi/a)$, and $\tilde{\mathcal{I}}_2(10\pi/a)$. The first, $\tilde{\mathcal{I}}_2(0)$, is necessarily real and without loss of generality. We may define the second, $\tilde{\mathcal{I}}_2(2\pi/a)$, to be real as well, because the phase may be removed by translation. The rest of these Fourier components may have nonzero phases, and thus we are left with the problem of maximizing $\gamma_1(\varepsilon)$ over a ten-dimensional parameter space. This space is highly restricted by using the Rearrangement, Parseval, and Toeplitz realizability conditions on the Fourier components listed above. The optimization is performed with a reliable interior-point optimization method,[26]

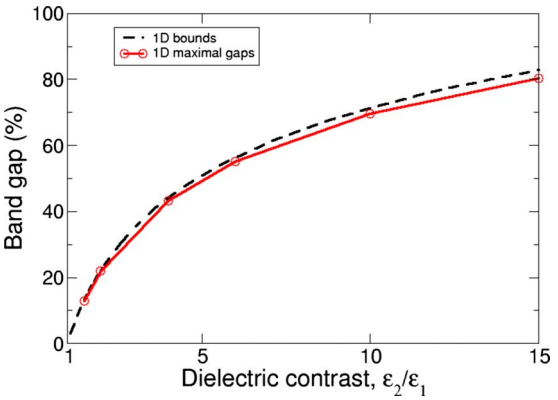

FIG. 6. (Color online) Upper bounds on the one-dimensional photonic band gap (black dashed line), as a function of dielectric contrast, as derived in Sec. V of this paper. The solid red line gives the largest band gap obtained for any one-dimensional unit-cell configuration. This is the simplest possible one-dimensional structure: a single interval of phase 2 in a background of phase 1, referred to in the text as the simple two-scale periodic geometry. Note that these are bounds over all possible volume fractions of phase 2.

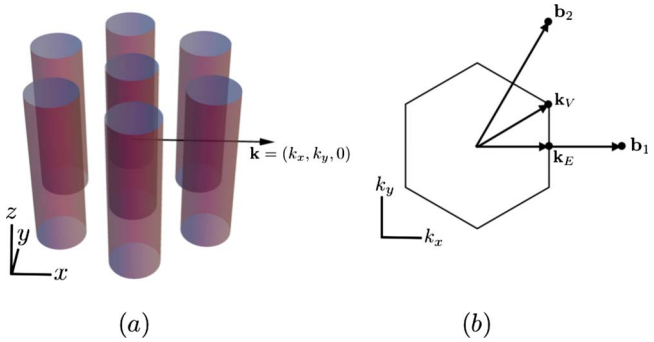

FIG. 7. (Color online) Part (a) is a schematic depiction of a two-dimensional photonic crystal. The cylinders extend infinitely in the z direction, propagation is confined to the x-y plane, and the magnetic field may polarized in the x-y plane (TM case) or in the z direction (TE case). The structure shown is an example of one with sixfold rotational symmetry, with one cylinder in each hexagonal unit cell. Part (b) is a depiction of the two-dimensional first Brillouin zone. We find upper and lower bounds for the frequency bands at both $\mathbf{k}_E$ and $\mathbf{k}_V$ in order to achieve a better bound on the complete band gap.

and thus the overall band-gap bound Γ_1 is obtained for any given dielectric contrast ratio, $\varepsilon_2/\varepsilon_1$.

The bounds are plotted in Fig. 6 as a function of $\varepsilon_2/\varepsilon_1$. Also plotted for the sake of comparison is the largest known one-dimensional band gap. This optimal structure is simply one contiguous interval of dielectric constant ε_2 in a background of dielectric constant ε_1 within the unit cell. We refer to this structure as the simple two-scale periodic geometry. To the authors' knowledge, there is no rigorous proof that this is the structure that yields the largest band gap; this is an indication of the difficulty of the problem. There is strong reason to believe that this yields the largest first band gap, however, since it leads to the most possible Bragg scattering at the first nonzero reciprocal lattice vector. The maximal band gap for each dielectric contrast ratio is obtained (using the MPB program[20]) by maximizing the gap with respect to the length of the interval. Note that the bounds approach the optimal structure as $\varepsilon_2/\varepsilon_1 \to 1$. We prove in the Appendix that this is true in a certain sense: at any Bloch wave vector, the lower and upper bounds converge in this limit. While this does not prove that the bounds are sharp (since there remains the possibility that a sufficient number of Bloch wave vectors have not been incorporated), it is highly suggestive that they are at least in the one-dimensional case.

VI. UPPER BOUNDS ON THE FIRST BAND GAP IN TWO DIMENSIONS

In this section, we present the method for and results of the calculation of upper bounds of the first band gap of the hexagonal and square lattices. In the hexagonal case, sixfold rotational symmetry (symmetry group C_6) is enforced, and in the square case, fourfold rotational symmetry (symmetry group C_4) is enforced. These constraints on the optimization are well motivated, since when hexagonal and square unit cells are used, numerical calculations have shown that the maximum-band-gap structures (for many different band gaps in the spectrum) have sixfold and fourfold rotational symmetry, respectively. Figure 7 shows an example of a two-dimensional hexagonal photonic crystal. This is a structure whose dielectric constant is purely a function of two Cartesian coordinates, (x,y), and is independent of the third (z), thus, $\varepsilon(\mathbf{x}) \to \varepsilon(x,y)$. We thus consider Bloch wave vectors in the plane, so that $\mathbf{k}=(k_x,k_y,0) \to (k_x,k_y)$. Also shown in Fig. 7 is the two-dimensional Brillouin zone of this structure, with two Bloch wave vectors at high symmetry points labeled, namely $\mathbf{k}_E$ and $\mathbf{k}_V$; both of these were used in the calculation of the band-gap bounds. We derive band-gap bounds for both the TM and TE cases, where the magnetic field is polarized in the (x,y) plane in the former and perpendicular to the plane in the latter (vice versa for the electric field), respectively.

A. Band-gap bounds for the hexagonal lattice

Here, we calculate upper bounds for the first band gap of the hexagonal lattice defined by the direct lattice vectors $\mathbf{a}_1 = a(1,-1/\sqrt{3})$ and $\mathbf{a}_2 = a(0,2/\sqrt{3})$ [and with reciprocal lattice vectors given by $\mathbf{b}_1 = (2\pi/a)(1,0)$ and $\mathbf{b}_2 = (2\pi/a)(1/2,\sqrt{3}/2)$]. We obtain upper and lower bounds on the frequency bands at the two Bloch wave vectors $\mathbf{k}_E = (\pi/a,0)$ and $\mathbf{k}_V = (\pi/a,\pi/\sqrt{3}a)$, as depicted in Fig. 7. As in the one-dimensional case, we use plane-wave trial wave functions. At $\mathbf{k}_E$, the center of a zone edge, we choose four such plane waves, with wave vectors $\mathbf{G}=(0,0)$, $(-2\pi/a,0)$, $(\pi/a,\sqrt{3}\pi/a)$, and $(-\pi/a,-\sqrt{3}\pi/a)$. At $\mathbf{k}_V$, a zone vertex, we choose six plane-wave trial wave functions, with wave vectors $\mathbf{G}=(0,0)$, $(-2\pi/a,0)$, $(-\pi/a,-\sqrt{3}\pi/a)$, $(-\pi/a, \sqrt{3}\pi/a)$, $(-3\pi/a,-\sqrt{3}\pi/a)$, and $(\pi/a,-\sqrt{3}\pi/a)$.

To calculate upper bounds on the frequency bands, we use the procedure described in Sec. III A and define the polarizations of our plane-wave trial wave functions as follows. In the TE case, they are polarized in the z direction and we use

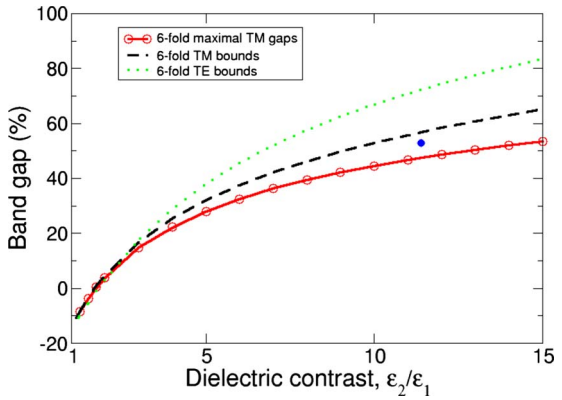

FIG. 8. (Color online) Upper bounds on the first two-dimensional TM photonic band gap (black dashed line), and upper bounds on the first two-dimensional TE photonic band gap (green dotted line), both with imposed sixfold rotational symmetry, plotted as a function of dielectric contrast. The red solid line gives the largest known TM band gaps as a function of dielectric contrast (Ref. 14). The blue circle denotes the largest realized first TE band gap (52%), at dielectric contrast 11.56 (from Ref. 13). Note that these are bounds over all possible volume fractions of phase 2.

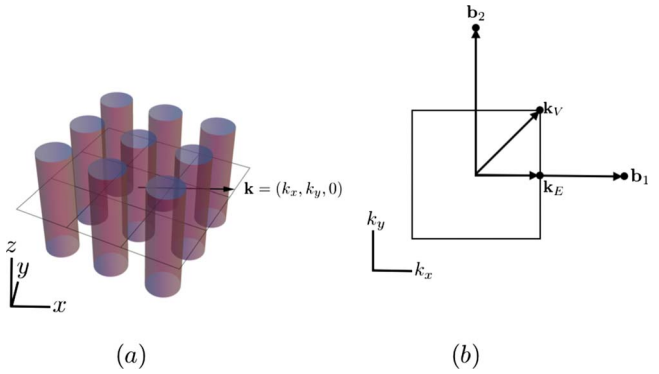

FIG. 9. (Color online) Part (a) is a schematic depiction of a two-dimensional photonic crystal with fourfold (C_4) symmetry. The cylinders extend infinitely in the z direction, propagation is confined to the x-y plane, and the magnetic field may polarized in the x-y plane (TM case) or in the z direction (TE case). Part (b) is a depiction of the two-dimensional square first Brillouin zone. We find upper and lower bounds for the frequency bands at both $\mathbf{k}_E$ and $\mathbf{k}_V$ in order to achieve a better bound on the complete band gap.

the magnetic field wave equation to obtain the upper bounds (since in the TE polarization, the magnetic field is perpendicular to the plane). We cannot use the electric field wave equation for the TE polarization because plane waves polarized in plane do not satisfy the no-free-charge condition, Eq. (6), and thus may not be used as trial functions within the space $\mathcal{P}^E_{\mathbf{k}}$, for any $\mathbf{k}$. In the TM case, we may use both the magnetic and electric field wave equations to obtain upper bounds on the frequency bands. For the former, the trial functions are polarized in plane, transverse to the direction of propagation, $\mathbf{k}+\mathbf{G}$ (and thus satisfy the transversality constraint). For the latter, trial wave functions are polarized in the z direction (these therefore satisfy the no-free-charge constraint and are orthogonal with respect to the dielectric function ε). Note that these two upper bounds may be used together to find a lower upper bounds on the frequency bands. To bound the first band gap, we use only the upper bound on the second frequency band. To calculate lower bounds on the frequency bands, we use the procedure described in Sec. III B. The plane-wave trial wave functions are polarized in plane for the TM case, and in the z direction for the TE case.

As in the one-dimensional case, the expression for $\gamma_1(\varepsilon)$ implicitly contains a number of the Fourier components of the indicator function $\mathcal{I}_2$. They are $\tilde{\mathcal{I}}_2((0,0))$, $\tilde{\mathcal{I}}_2((2\pi/a,0))$, $\tilde{\mathcal{I}}_2((0,2\sqrt{3}\pi/a))$, and $\tilde{\mathcal{I}}_2((4\pi/a,0))$. Each of the latter three Fourier components are equal to five others by the C_6 symmetry operations, each defining a ring of reciprocal lattice vectors. Since the inversion operation is contained in C_6, these components must be real. We perform a numerical maximization of $\gamma_1(\varepsilon)$ with respect to these four parameters subject to the realizability conditions defined in Sec. IV.

The bounds on the first TE and TM band gaps with the hexagonal lattice configuration are presented in Fig. 8, plotted as a function of the dielectric contrast ratio, namely $\varepsilon_2/\varepsilon_1=11.56$. For comparison, the largest known band gaps for this system are plotted in the same figure. The TM and TE maximized band gaps were taken from Refs. 13 and 14, respectively, however, in the TE case the optimization was only performed at a single value of the contrast ratio. Similarly to the one-dimensional case, the maximized band gaps converge to the bounds in the limit $\varepsilon_2/\varepsilon_1 \to 1$. In this limit the bounds may be thought of as sharp in the sense that at any Bloch wave vector $\mathbf{k}$, the lower and upper bounds converge to first order in $\varepsilon_2/\varepsilon_1-1$, as shown in the Appendix.

B. Band-gap bounds for the square lattice

The calculation of the band-gap bounds for the square lattice, with C_4 symmetry enforced proceeds completely analogously to the sixfold case, with the only change being the choice of Bloch wave vectors and trial wave functions. Figure 9 depicts a two-dimensional photonic crystal with fourfold symmetry and a square unit cell. It also shows the two-dimensional Brillouin zone with two points of high symmetry at $\mathbf{k}_E$ and $\mathbf{k}_V$. As in the hexagonal case, we use both of these points to bound the band gap. In the square case, with direct lattice vectors $\mathbf{a}_1=a(1,0)$ and $\mathbf{a}_2=a(0,1)$, and reciprocal lattice vectors $\mathbf{b}_1=(2\pi/a)(1,0)$ and $\mathbf{b}_2=(2\pi/a)(0,1)$, we have that $\mathbf{k}_E=(\pi/a)(1,0)$ and $\mathbf{k}_V=(\pi/a)(1,1)$.

In the calculation of the upper and lower bounds on the frequency bands at $\mathbf{k}_E$, we use two plane-wave trial wave functions with wave vectors given by $\mathbf{G}=(0,0)$ and $\mathbf{G}=(-2\pi/a,0)$. At $\mathbf{k}_V$, we use four plane-wave trial wave functions at $\mathbf{G}=(0,0)$, $(-2\pi/a,0)$, $(0,-2\pi/a)$ and $\mathbf{G}=(-2\pi/a, -2\pi/a)$. The polarizations of these plane waves are chosen in exact analogy with the sixfold case for both the TM and TE polarizations. The bounds on the band gap for the fourfold case are plotted in Fig. 10, as a function of $\varepsilon_2/\varepsilon_1$. For comparison, we have also plotted the maximum achieved band gap for any structure in both polarizations (taken from Ref. 14 for a range $\varepsilon_2/\varepsilon_1$ and from Ref. 13 for $\varepsilon_2/\varepsilon_1=11.56$).

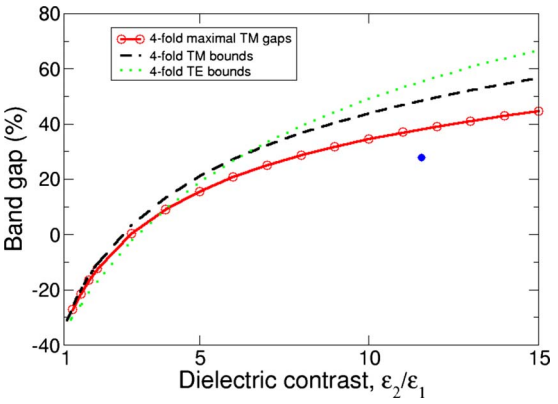

FIG. 10. (Color online) Upper bounds on the first two-dimensional TM photonic band gap (black dashed line), and upper bounds on the first two-dimensional TE photonic band gap (green dotted line), both with imposed fourfold rotational symmetry, plotted as a function of dielectric contrast. The red solid line gives the largest known TM band gaps as a function of dielectric contrast (Ref. 14). The blue circle denotes the largest realized first TE band gap ~(29%), at dielectric contrast 11.56 (from Ref. 13). Note that these are bounds over all possible volume fractions of phase 2.

VII. CONCLUSIONS

In this paper, we have proposed a general method to find upper bounds on band gaps of two-component photonic crystals. We applied the technique to a one-dimensional photonic crystal, two-dimensional photonic crystals with sixfold rotational symmetry, and those with fourfold rotational symmetry. In all cases, we found bounds on the first band gap that were extremely tight for low dielectric contrasts (as compared with the maximal band gaps that may be achieved), and then diverged slowly as contrast increased. To summarize the method itself, we used the Rayleigh-Ritz procedure to calculate upper bounds on the frequency bands, the method of intermediate problems to calculate lower bounds, and used plane-wave trial wave functions for both of them. Taken together, these gave a bound on the band gap, $\gamma_1(\varepsilon)$, for any given structure. To find the bound on the band gap over all structures, we had to maximize $\gamma_1(\varepsilon)$ over all possible two-component structures. We found that since plane-wave trial functions were used, the only structural parameters that entered into the calculation of $\gamma_1(\varepsilon)$ were a finite number of Fourier coefficients of the indicator function for one of the phases (chosen arbitrarily to be phase 2). By maximizing over all *realizable* values of the corresponding Fourier components (i.e., those values that are possible to give rise to an indicator function in real space), we obtained the overall bound on the band gap, for any given dielectric contrast. In another paper,[16] we will introduce band-gap bounds in three dimensions.

The method used here does not lend itself to calculating bounds on photonic band gaps in quasicrystalline or amorphous systems, since we require that the structure be periodic and therefore that the Bloch theorem applies.

We have limited ourselves in this paper to the calculation of bounds on the first photonic band gap, but the method is straightforwardly generalized to calculate higher band gaps in the spectrum. That said, the first band gap in one- and two-dimensional systems is by far the most studied, both experimentally and theoretically. Furthermore, as it has been argued previously that higher band gaps are much less robust against fabrication imperfections.[27]

There has been extensive work on finding upper and lower bounds for the effective dielectric constant of multicomponent disordered systems.[19] These bounds may be expressed in terms of n-point correlation functions of the disordered structure, where the bounds improve as more correlation information is included. In the present work, since bounds are first derived in terms of Fourier components of indicator functions, their is no immediate parallel with bounds derived in terms of correlation functions. To be more specific, consider the two-point correlation function of a two-component structure. It implicitly contains information about the amplitudes of the Fourier components, but not their phases. Since in the present work we incorporate phase information, these bounds cannot be expressed purely in terms of the standard two-point correlation (autocorrelation function involving the indicator function).

In future work, we will extend the present analysis to obtain upper and lower bounds on the eigenvalues of the Laplacian operator, which is a simpler problem. Such eigenvalues are of direct relevance to the determination of the relaxation times associated with diffusion and reaction in fluid-saturated porous media as well as nuclear magnetic relaxation in such media.[19,28,29] However, the development of bounds on the eigenvalues (inversely proportional to the relaxation times) has been very limited. For example, the Rayleigh-Ritz formulation has only been used to get lower bounds on the largest relaxation time (smallest positive eigenvalue).[28] Upper bounds have not been obtained for the largest relaxation time and no bounds exist for any of the other eigenvalues. We intend to provide such bounds in the future.

ACKNOWLEDGMENTS

M.C.R. acknowledges useful discussions with C. Sinan Gunturk, Bob Kohn, and Marian Florescu. S.T. acknowledges National Science Foundation support under Grant No. DMR-0606415.

APPENDIX: SHARPNESS OF BOUNDS IN THE LOW-CONTRAST LIMIT

In this Appendix, we prove that in the limit of low dielectric contrast, the lower bounds and upper bounds (derived using plane-wave trial functions) on the bands at any given **k** approach one another. Although this does not prove that the largest-band-gap structure realizes the bounds in this limit, it strongly suggests that if a sufficient number of **k**'s are used in calculating the bound, the bound will be achieved by some structure. It also accounts for why, in Figs. 6 and 8, the maximum-band-gap structure approaches the bound in the limit of low contrast.

In order to prove this, we will need the following identity: given square matrix P with matrix elements of the form

$$P_{ij} = \alpha_i \delta_{ij} + \beta_{ij}\Delta + \mathcal{O}(\Delta^2), \tag{37}$$

where δ_{ij} is the Kronecker delta, Δ is a small expansion parameter, and $i,j \in \{1,\ldots,n\}$, then the matrix elements of the inverse of this matrix are

$$P_{ij}^{-1} = \frac{1}{\alpha_i}\delta_{ij} - \frac{\beta_{ij}}{\alpha_i \alpha_j}\Delta + \mathcal{O}(\Delta^2). \tag{38}$$

Now, to prove the equality of the upper and lower bounds in the low contrast limit, it is sufficient to show that

$$U^H_{(\mathbf{G}'\lambda')(\mathbf{G}\lambda)} = \frac{|\mathbf{k}+\mathbf{G}|^2}{\varepsilon_0}\delta_{(\mathbf{G}'\lambda')(\mathbf{G}\lambda)} + M^{-1}_{(\mathbf{G}'\lambda')(\mathbf{G}\lambda)}, \tag{39}$$

where all of the quantities here are defined in Eqs. (11) and (16)–(18). Recall that the reciprocal lattice vector $\mathbf{G}$ and polarization index $\lambda \in \{1,2\}$ taken together index a single plane-wave basis member.

We first re-express the left-hand side of Eq. (39) using Eq. (11) as

$$U^H_{(\mathbf{G}'\lambda')(\mathbf{G}\lambda)} = [(\mathbf{k}+\mathbf{G}') \times \hat{\mathbf{e}}_{\mathbf{k}+\mathbf{G}',\lambda'}] \cdot [(\mathbf{k}+\mathbf{G}) \times \hat{\mathbf{e}}_{\mathbf{k}+\mathbf{G},\lambda}] \times [\eta_1 + (\eta_2 - \eta_1)\tilde{\mathcal{I}}_2(\mathbf{G}-\mathbf{G}')], \tag{40}$$

where $\eta_i = 1/\varepsilon_i$ for $i \in \{1,2,3\}$. We will show that in the limit of low contrast, i.e., $\varepsilon_2/\varepsilon_1 \to 1$, the right-hand side of Eq. (39) is equal to this to first order in the expansion parameter $\Delta\eta = \eta_2 - \eta_1$.

Consider the expression given in Eq. (18) for the matrix element of M.

$$M_{(\mathbf{G}'\lambda')(\mathbf{G}\lambda)} = \frac{[(\mathbf{k}+\mathbf{G}') \times \hat{\mathbf{e}}_{\mathbf{k}+\mathbf{G}',\lambda'}] \cdot [(\mathbf{k}+\mathbf{G}) \times \hat{\mathbf{e}}_{\mathbf{k}+\mathbf{G},\lambda}]}{|\mathbf{k}+\mathbf{G}'|^2 |\mathbf{k}+\mathbf{G}|^2} \times \{(\eta_1 - \eta_0)^{-1} + [(\eta_2 - \eta_0)^{-1} - (\eta_1 - \eta_0)^{-1}]\tilde{\mathcal{I}}_2(\mathbf{G}-\mathbf{G}')\}, \tag{41}$$

but we may make the following expansion:

$$[(\eta_2 - \eta_0)^{-1} - (\eta_1 - \eta_0)^{-1}] = \frac{-\Delta\eta}{(\eta_1 - \eta_0)^2} + \mathcal{O}(\Delta\eta^2). \tag{42}$$

Thus, the matrix M is of the form of P, and we may use the identity derived earlier in this Appendix to obtain the inverse of M to first order in $\Delta\eta$

$$M^{-1}_{(\mathbf{G}'\lambda')(\mathbf{G}\lambda)} = |\mathbf{k}+\mathbf{G}|^2(\eta_1 - \eta_0)\delta_{(\mathbf{G}'\lambda')(\mathbf{G}\lambda)} + [(\mathbf{k}+\mathbf{G}') \times \hat{\mathbf{e}}_{\mathbf{k}+\mathbf{G}',\lambda'}] \cdot [(\mathbf{k}+\mathbf{G}) \times \hat{\mathbf{e}}_{\mathbf{k}+\mathbf{G},\lambda}] \times (\eta_2 - \eta_1)\tilde{\mathcal{I}}_2(\mathbf{G}-\mathbf{G}'). \tag{43}$$

Comparing this to Eq. (39) completes the proof.

[1] S. John, Phys. Rev. Lett. **58**, 2486 (1987).
[2] E. Yablonovitch, Phys. Rev. Lett. **58**, 2059 (1987).
[3] For one-dimensional structures (i.e., those that are periodic in one dimension and extend infinitely in the other two), we limit the propagation direction to that in which the structure is periodic, for the purpose of defining a *complete* band gap. For two-dimensional systems (those that are two-dimensionally periodic and extend infinitely in the other direction), we limit the propagation direction to be in the plane of periodicity. The transverse-magnetic and transverse-electric polarizations in two dimensions are considered separately, so that a band gap may be considered complete independently for these two cases.
[4] A. Mekis, J. C. Chen, I. Kurland, S. Fan, P. R. Villeneuve, and J. D. Joannopoulos, Phys. Rev. Lett. **77**, 3787 (1996).
[5] B. Temelkuran, S. D. Hart, G. Benoit, J. D. Joannopoulos, and Y. Fink, Nature (London) **420**, 650 (2002).
[6] S. John and M. Florescu, J. Opt. A, Pure Appl. Opt. **3**, S103 (2001).
[7] K. M. Ho, C. T. Chan, and C. M. Soukoulis, Phys. Rev. Lett. **65**, 3152 (1990).
[8] E. Yablonovitch, T. J. Gmitter, and K. M. Leung, Phys. Rev. Lett. **67**, 2295 (1991).
[9] K. M. Ho, C. T. Chan, C. M. Soukoulis, R. Biswas, and M. Sigalas, Solid State Commun. **89**, 413 (1994).
[10] M. Maldovan and E. L. Thomas, Nature Mater. **3**, 593 (2004).
[11] M. Maldovan, C. K. Ullal, W. C. Carter, and E. L. Thomas, Nature Mater. **2**, 664 (2003).
[12] C. Y. Kao, S. Osher, and E. Yablonovitch, Appl. Phys. B: Lasers Opt. **81**, 235 (2005).
[13] O. Sigmund and K. Hougaard, Phys. Rev. Lett. **100**, 153904 (2008).
[14] M. C. Rechtsman, H. C. Jeong, P. M. Chaikin, S. Torquato, and P. J. Steinhardt, Phys. Rev. Lett. **101**, 073902 (2008).
[15] Three-dimensional maximization of the band gap with respect to the dielectric structure is computationally intensive due to the high cost of calculating photonic band structure using the plane-wave expansion method (Ref. 20).
[16] M. C. Rechtsman and S. Torquato (unpublished).
[17] B. N. Parlett, *The Symmetric Eigenvalue Problem* (Prentice-Hall, Englewood Cliffs, NJ, 1998).
[18] A. Weinstein and W. Stenger, *Methods of Intermediate Problems for Eigenvalues: Theory and Ramifications* (Academic, New York, 1972).
[19] S. Torquato, *Random Heterogeneous Materials* (Springer, New York, 2002).
[20] S. Johnson and J. Joannopoulos, Opt. Express **8**, 173 (2001).
[21] S. R. Vatsya and S. K. Nikumb, Phys. Rev. B **66**, 085102 (2002).
[22] S. Torquato, Ind. Eng. Chem. Res. **45**, 6923 (2006).
[23] L. A. Shepp, Proceedings of the Working Conference on the Stochastic Process, Santa Barbara, CA (unpublished), pp. 205–218.
[24] E. H. Lieb and M. Loss, *Analysis* (American Mathematical Society, Providence, 2001).
[25] R. M. Gray, *Toeplitz and Circulant Matrices: A Review* (Now, Delft, 2006).
[26] D. G. Luenberger and Y. Ye, *Linear and Nonlinear Programming* (Springer, New York, 2008).
[27] Z. Y. Li and Z. Q. Zhang, Phys. Rev. B **62**, 1516 (2000).
[28] S. Torquato and M. Avellaneda, J. Chem. Phys. **95**, 6477 (1991).
[29] S. Torquato and I. C. Kim, J. Appl. Phys. **72**, 2612 (1992).